Journal for ImmunoTherapy of Cancer

Preclinical optimization of a GPC2-targeting CAR T-cell therapy for neuroblastoma

Ming Sun,[1] Yingying Cao,[2] Reona Okada,[1] Jeyshka M Reyes-González,[1] Hannah G Stack,[1] Haiying Qin,[1] Nan Li,[3] Charlie Seibert,[4] Michael C Kelly,[5] Eytan Ruppin ,[2] Mitchell Ho,[3] Carol J Thiele,[1] Rosa Nguyen [1]

To cite: Sun M, Cao Y, Okada R, *et al*. Preclinical optimization of a GPC2-targeting CAR T-cell therapy for neuroblastoma. *Journal for ImmunoTherapy of Cancer* 2023;**11**:e005881. doi:10.1136/jitc-2022-005881

► Additional supplemental material is published online only. To view, please visit the journal online (http://dx.doi.org/10.1136/jitc-2022-005881).

Accepted 30 December 2022

[1]Pediatric Oncology Branch, NCI, Bethesda, Maryland, USA
[2]Cancer Data Science Laboratory, NCI, Bethesda, Maryland, USA
[3]Laboratory of Molecular Biology, National Institutes of Health, Bethesda, Maryland, USA
[4]Center for Cancer Research Single Cell Analysis Facility, Frederick National Laboratory for Cancer Research, Frederick, Maryland, USA
[5]Single Cell Analysis Facility, Center for Cancer Research, National Cancer Institute, Bethesda, Maryland, USA

Correspondence to
Dr Rosa Nguyen;
hongharosa.nguyen@nih.gov

ABSTRACT

Background Although most patients with newly diagnosed high-risk neuroblastoma (NB) achieve remission after initial therapy, more than 50% experience late relapses caused by minimal residual disease (MRD) and succumb to their cancer. Therapeutic strategies to target MRD may benefit these children. We developed a new chimeric antigen receptor (CAR) targeting glypican-2 (GPC2) and conducted iterative preclinical engineering of the CAR structure to maximize its anti-tumor efficacy before clinical translation.

Methods We evaluated different GPC2-CAR constructs by measuring the CAR activity in vitro. NOD-SCID mice engrafted orthotopically with human NB cell lines or patient-derived xenografts and treated with human CAR T cells served as in vivo models. Mechanistic studies were performed using single-cell RNA-sequencing.

Results Applying stringent in vitro assays and orthotopic in vivo NB models, we demonstrated that our single-chain variable fragment, CT3, integrated into a CAR vector with a CD28 hinge, CD28 transmembrane, and 4-1BB co-stimulatory domain (CT3.28H.BBζ) elicits the best preclinical anti-NB activity compared with other tested CAR constructs. This enhanced activity was associated with an enrichment of $CD8^+$ effector T cells in the tumor-microenvironment and upregulation of several effector molecules such as *GNLY*, *GZMB*, *ZNF683*, and *HMGN2*. Finally, we also showed that the CT3.28H.BBζ CAR we developed was more potent than a recently clinically tested GD2-targeted CAR to control NB growth in vivo.

Conclusion Given the robust preclinical activity of CT3.28H.BBζ, these results form a promising basis for further clinical testing in children with NB.

WHAT IS ALREADY KNOWN ON THIS TOPIC

⇒ The lack of tumor-associated antigens in solid tumors has impeded the development of effective and safe chimeric antigen receptor (CAR) T-cell therapies.

WHAT THIS STUDY ADDS

⇒ We have developed a CAR T therapy against a new immunotherapy target called glypican-2 for children with neuroblastoma.

HOW THIS STUDY MIGHT AFFECT RESEARCH, PRACTICE OR POLICY

⇒ Given the robust preclinical activity of CT3.28H.BBζ, we will conduct a Phase I/II clinical trial administering this CAR T-cell therapy for the first time to pediatric patients with relapsed/refractory neuroblastoma. This trial will be supported by the National Cancer Institute Cancer Moonshot Initiative.

INTRODUCTION

High-risk neuroblastoma (NB) is a common pediatric cancer.[1] Although most patients with newly diagnosed high-risk NB achieve remission after multimodal therapy, more than 50% of these children experience late relapses caused by minimal residual disease (MRD) and succumb to their cancer.[2] A recent study demonstrated that the 5-year overall survival rate of these patients was improved by almost 20% with the incorporation of antibody therapy with cytokines to target MRD.[3] Despite this, one-third of all children still succumb to their cancer and need more efficacious treatments. Considering the past successes of chimeric antigen receptor (CAR) T-cell therapy against MRD in pediatric patients with hematologic malignancies,[4 5] several CAR T-cell therapies are now being actively developed for patients with NB. However, in general, CAR T-cell therapy has been less effective in solid tumors, including NB, than in leukemias.[4–7] This is demonstrated by the results of the first GD2-targeted CAR T trials in the relapsed patient population with NB.[7–11] Only 3 of the cumulative 42 patients with active disease across four trials who received either 14.18 or K666 single-chain variable fragment (scFv)-based GD2-CAR T cells achieved sustained objective responses.[7 9–11]

A critical impediment to progress in CAR development for NB is the scarcity of tumor-specific targets. Ideally, the CAR target is expressed exclusively in tumor cells and

absent or present at only very low levels in normal cells so that treatment eliminates tumor cells but does not cause toxicity to healthy tissues. In recent years, CAR T-cell targets like B7H3,[12] ALK,[13] NCAM-1,[14] L1CAM,[15] and glypican-2 (GPC2)[16–20] have gained traction in preclinical studies as they fulfill this condition. Our group has focused on the preclinical development and clinical translation of GPC2-targeted CAR T-cell therapy for patients with NB.[19 20]

GPC2 is an antigen expressed during early fetal development after which it is largely silenced in normal tissue.[16 21] However, it is also expressed in NB, which renders it an ideal target for immunotherapy. The expression levels of GPC2 as compared with other CAR targets like GD2 (~100-fold higher) and B7H3 (~5-fold higher) is very low in NB.[17] This has implications for the effectiveness of the CAR because lower antigen density is associated with lower CAR engagement, activation, and antitumor activity.[22] Thus, we conducted preclinical optimization of the CAR structure through iterative engineering to maximize its antitumor efficacy before clinical translation. We applied in vitro and in vivo models to show that our anti-GPC2 scFv (CT3) with a CD28 hinge, CD28 transmembrane (TM), and 4-1BB co-stimulatory domain elicits the best preclinical anti-NB activity across three different GPC2-CAR constructs. In addition, we compared the antitumor activity of the CT3.28H.BBζ CAR with that of a recently clinically tested GD2 CAR using the identical backbone CAR construct.[7] Our functional results correlate with transcriptomic differences captured by single-cell RNA-sequencing (seq) and, altogether, justify the clinical translation of CT3.28H.BBζ CAR T-cell therapy for patients with NB.

METHODS

Cell lines

The drug-resistant patient-derived xenograft (PDX) SJNBL012407_X1 (*MYCN*-amplified) was provided by the Children's Solid Tumor Network. IMR-5, CHP-212, SK-N-BE2C, Kelly (also *MYCN*-amplified) and SHIN, SK-N-FI, SK-N-AS, SH-SHEP, and SH-SY5Y (*MYCN*-wildtype (WT)) were retrieved from the National Cancer Institute (NCI) Pediatric Oncology Branch cell line repository. NGP-GPC2^{hi}, NBSD-GPC2^{mod}, and SMS-SAN^{lo} (all *MYCN*-amplified) were kindly provided by Stanford. The GPC2 expression of all lines was determined (online supplemental figure 1). We confirmed that all cells were mycoplasma free. The cell identity was determined by short-tandem repeat DNA profiling. We generated stable luciferase (ffLUC)-green fluorescent protein (GFP)-expressing cells by lentiviral transduction and subsequent selection with 0.5 µg/mL of puromycin (Thermo Fisher Scientific). PDX cells were passaged in mice. The NB cell lines were grown in RPMI (Roswell Park Memorial Institute) medium supplemented with 10% fetal bovine serum (FBS) and 100 U/mL penicillin/streptomycin (Gibco).

CAR constructs

As previously described,[23] we cloned the CT3 scFv into the lentiviral vector, pWPT (Addgene #12255), and added different hinge and TM domains (either CD8 or CD28) and co-stimulatory domains (4-1BBζ and/or CD28) to generate variations of CAR T-cell constructs. The GD2 CAR sequence was retrieved from publicly available sources[7 24] and cloned into the pWPT vector containing a CD8 or CD28 hinge and TM as well as a 4-1BB co-stimulatory domain. A human truncated extracellular epidermal growth factor receptor domain (hEGFRt) was included as a tag and is recognized by cetuximab.

Human T cells and CAR transduction

Cryopreserved human T cells of healthy volunteer donors (National Institutes of Health Blood Bank) were used for CAR T-cell production as previously described.[23] Briefly, on Day 0, Lenti-X 293T cells were plated at a density of 2×10^7 cells per Poly-D-lysine-coated 15 cm dish and subsequently transfected with the CT3 CAR plasmid, envelope plasmid (pMD2.G), and packaging plasmid (psPAX2) at a ratio of 4:1:3 using Lipofectamine 2000 (Thermo Fisher Scientific). The lentivirus-containing supernatants of the Lenti-X 293T cultures were harvested 48–72 hours post-transfection and used to spin-transduce the human T cells. Cryopreserved human T cells were thawed and grown in AIM-V medium (Gibco) supplemented with 10% FBS (Omega Scientific), 100 U/mL penicillin/streptomycin, 1X non-essential amino acids, 0.2 mM L-GlutaMAX, 0.1 mM sodium pyruvate (all Gibco), CD3/CD28-coated Dynabeads (1:1 bead-to-cell ratio, Thermo Fisher Scientific), and 40 IU/mL interleukin (IL)-2 (NCI Frederick BRB Preclinical Repository). The IL-2 concentration was increased to 100 IU/mL after 48 hours at the time of lentiviral transduction. On Day 5 of T-cell culture, the Dynabeads were removed, and the transduced CAR T cells were expanded in culture until Day 8–10 for subsequent downstream assays.

CAR western blot assay

Manufactured CAR T cells were grown in culture for 3–5 hours while deprived of IL-2. To activate the CAR, either 1.7 µg of GPC2-Fc or 1 µg of Protein L (Acro Biosystems) was added to $2–3\times10^6$ cells in a 96-well-round-bottom plate and subsequently cross-linked at 37°C for varying times. Then, the cells were lysed using radioimmunoprecipitation assay (RIPA) buffer supplemented with Halt protease and phosphatase inhibitor cocktail (Thermo Fisher Scientific). A Bradford Assay (Bio-Rad Laboratories) was used to quantify the protein yields. Samples in the sodium dodecyl sulfate (SDS)-containing buffer were denatured for 10 min. A total of 5–10 µg of protein was resolved by 4–20% SDS-polyacrylamide gel electrophoresis (PAGE) and electroblotted onto a polyvinylidene difluoride membrane. The primary antibodies listed in online supplemental table 1 were incubated overnight at 4°C in 5% bovine serum albumine (BSA) in Tris-buffered saline

containing 0.1% Tween-20 (TBST) and 0.02% sodium azide. Secondary antibodies were incubated for 1 hour at room temperature in 5% non-fat dry milk in TBST. Protein bands were visualized using a goat anti-rabbit or anti-mouse IgG-HRP conjugated secondary antibody (200 µg/mL; Santa Cruz Biotechnology) and the SuperSignal West Femto Maximum Sensitivity Substrate (Thermo Fisher Scientific). Enhanced chemiluminescence (Bio-Rad Laboratories) was applied to visualize the bands, which were quantified with ImageJ.

In vitro cytotoxicity assays

CAR T cells and ffLUC-GFP-expressing NB tumor cells were co-cultured at varying effector-to-tumor (E:T) ratios as previously described.[25] Every 24 hours thereafter, the starting number of tumor cells was added to each well to re-challenge the CAR T cells. The specific lysis of the tumor cells was measured using the ONE-Glo assay. The results were normalized to conditions with untransduced (UT) mock T cells.

Mice

For all studies, 4–6 weeks old female NOD-SCID (NSG) mice were obtained from the NCI Center for Cancer Research Animal Resource Program. All studies were approved by the Institutional Animal Care and Use Committee.

Bioluminescence imaging

IMR-5 with stable expression of ffLUC was used for bioluminescence imaging (BLI). Tumor-bearing mice were injected with d-luciferin potassium salt (150 mg/kg, intraperitoneal (IP)) and imaged on an IVIS Lumina XR System (PerkinElmer) 5 min after d-luciferin injection (1 min acquisition time). Region of interest analysis was performed using the Living Image software (PerkinElmer; V.4.3.1).

In vivo therapy model

We implanted either PDX cells or IMR-5 orthotopically (2.5×10^5) into NSG mice.[23] Typically, 3 weeks after tumor implantation surgery, animals meeting enrollment criteria with a BLI (>10^7 photon/s), were randomized to receive either UT mock control T cells or GPC-targeted CAR T cells. The numbers of tail vein injected T cells were based on CAR^+ T cells. Total T cell numbers in mock groups were adjusted to match those in the CAR groups. For PDX studies, the experiment was terminated on Day 50 after tumor injection. Since BLI signals did not correlate with large tumor burdens, we recorded tumor weights at the end of the study to determine the treatment efficacy. For experiments with IMR-5, tumor-bearing animals were monitored via BLI. The survival of treated mice was monitored until Day 80 (~11 weeks since tumor implantation). Survival endpoints were death, >20% weight loss from baseline, or severe moribund status as determined by an animal caretaker, who was blinded to the study.

In vivo homing studies

Mice with IMR-5 WT NB were injected with ffLUC-GFP-expressing GPC2-targeting CAR T cells or UT mock T cells. After tail vein injection of the T cells, the animals were monitored serially via BLI to assess homing and expansion of the T cells in vivo. At the end of the experiments, organs of luciferin-injected mice were removed at 5 min and imaged in 6-well Petri dishes.

Flow cytometry

Samples were stained using 1×10^6 cells. Gates were drawn with fluorescence-minus-one controls. Compensations and voltages were set with single-color controls. The following antibodies were used for the detection of surface epitopes: CD45 (detected by clone HI-30), CD3 (OKT3), CD4 (OKT4), and CD8 (HIT8a). GPC2-F_C and anti-human F_C (M1310G05) or anti-EGFR antibody (AY13) were used to measure CAR transduction efficiency. CT3 antibody (produced in Dr Mitchell Ho's laboratory) and anti-mouse IgG1 (RMG1-1) were used to detect GPC2 expression in tumor cells. The PE Phycoerythrin Fluorescence Quantitation Kit (BD) was used to determine the density of GPC2 expression as per the manufacturer's instructions. Data were collected on a Fortessa LSR machine. Data analysis was conducted with FlowJo V.10.

Cytokine bead assay

Cytokine bead assays (CBAs) were conducted to quantitate the secreted cytokines in the supernatant of T and tumor co-cultures following the manufacturer's instructions (BioLegend).

Single-cell RNA-seq

Two donors were used to manufacture CAR T cells, which we injected into IMR-5-bearing mice on Day 8 of cell manufacturing. The injection cell product was stained with TotalSeq-C antibodies targeting CD8 (cat. # 344752) and CD4 (cat. # 300567) and subjected to the 10X Genomics 5' V.3.1 chemistry kit for library generation. Eight days after T cell injection into the mice, tumors were processed into single-cell suspensions with viability >80%. Three tumor samples per treatment group were pooled. About 10,000 cells per group were loaded to capture 6000 cells. The complementary DNA libraries were sequenced on the Illumina NextSeq 2000 and NovaSeq 6000 with a target depth of approximately 50,000 reads per cell.

Computational analysis

Single-cell RNA-seq FASTQ files were processed using the CellRanger software suite (V.6.1.2, 10X Genomics) with the corresponding human GRCh38 genome reference. Custom reference (GRCh38+GFP) was used to see if GFP sequences were detected in annotated tumor cells. Cell barcodes were determined based on the distribution of unique molecular identifier (UMI) counts, and a filtered gene-barcode matrix was generated by CellRanger for the downstream analysis in Seurat (V.4.0.1, R package).[26 27] Cells with low (<200 genes) and greater

than 10% of UMIs mapped to mitochondrial genes were removed. Data integration across different samples and treatment groups was performed with reciprocal principal component analysis[28] implemented in Seurat. The 'NormalizeData' function with parameters: normalization.method = 'LogNormalize' and scale.factor=10,000 was applied to normalize the expression level of genes in each cell. The 'FindVariableFeatures' function with the 'vst' method was used to identify 2000 highly variable genes. The 'ScaleData' function with default parameters was used to scale and center gene expression matrices. To perform clustering, PCA dimensionality reduction was first conducted with the 'RunPCA' function. The first 20 principal components were selected to construct the shared nearest neighbor graph with the 'FindNeighbors' function. Clusters were determined using the Louvain algorithm with the 'FindClusters' function. SingleR (V.1.8.1, R package)[29] was used to do an initial automatic cell type annotation with the known cell type labels from the Blueprint/ENCODE reference and Database of Immune Cell Expression to predict the identities of cell clusters. Then, we manually checked whether the annotations were reliable by examining the top-ranked differentially expressed genes of each cluster, which were obtained with the 'FindAllMarkers' function with default parameters but with set min.pct=0.25. The uniform manifold approximation and projection (UMAP) was finally applied to visualize the single-cell transcriptional profiles in two-dimensional space. Tumor cells were confirmed by the GFP sequence and copy number variation analysis with infercnv (V.1.10.1, R package).[30] $CD45^+$ immune cells were annotated using canonical gene markers. Lymphoid cells were separated from tumor and mouse cells and reclustered to obtain more refined cell clusters. Differential gene expression was calculated for all pairs of clusters and therapy groups. Sample integration across the treatment groups was performed with the standard anchor-based workflow in Seurat. For initial clustering and annotation, we applied k-nearest neighbor (KNN) graph-based clustering on the weighted RNA similarities, to calculate the Jaccard index (neighborhood overlap) between every pair of cells with a high resolution and merging of clusters. UMAP plots were used to visualize the results using the Seurat package. Tumor cells were confirmed by the green fluorescent protein sequence and copy number variation analysis. $CD45^+$ immune cells were annotated using canonical gene markers. QIAGEN Ingenuity Pathway Analysis was used for pathway enrichment analysis (QIAGEN, https://digitalinsights.qiagen.com/IPA).[31]

Statistical analysis

The Student's t-test (normally distributed data) or Mann-Whitney U test (skewed data) were used to compare two groups and one-way analysis of variance (ANOVA, normally distributed data) followed by Tukey's post hoc comparison tests or a one-way ANOVA on ranks (skewed data) followed by the Dunn test for comparisons with more than two groups. For survival analysis, Kaplan-Meier curves were generated, and a two-sided log-rank test was used to compare survival between the groups. All experiments were performed in biological replicates with at least two donors.

Data availability

Data are available from the corresponding author on reasonable written request. The single-cell RNA-seq data were deposited in GEO (GSE212658).

RESULTS

In vitro comparison of CT3.28H.BBζ, CT3.8H.BBζ, and CT3.8H.28BBζ

To identify the most efficacious GPC2-CAR construct for clinical translation, we first performed a head-to-head comparison in vitro using CT3 in three different CAR backbone constructs (figure 1A; online supplemental figure 2): (1) CT3 with a CD8 hinge, CD8 TM, and 4-1BB costimulatory domain (CT3.8H.BBζ, published CAR),[19] (2) CT3 with a CD28 hinge, CD28 TM, and 4-1BB costimulatory domain (CT3.28H.BBζ), and (3) CT3 with a CD8 hinge, CD28 TM, and CD28-4-1BB costimulatory domain (CT3.8H.28BBζ). In co-culture with GPC2-WT or GPC2-knock out (KO) IMR-5 tumor cells, all three constructs showed increased levels of interferon-γ, granzyme B (GZMB), and soluble Fas ligand in the supernatant in the presence of the CAR antigen, GPC2 (figure 1B). The cytokine levels approximated background levels in conditions containing GPC2-KO cells, indicating specificity of the CARs. However, of the three constructs, we found that CT3.28H.BBζ demonstrated the least tonic signaling indicated by low phosphorylation levels of the CAR and downstream molecules such as ZAP70 or ERK at rest (figure 1C,D) but an appropriate increase thereof on CAR crosslinking in vitro. Although CT3.8H.BBζ also showed low tonic signaling at rest, the CAR activation was not as robust as with CT3.28H.BBζ after antigen-specific crosslinking. Furthermore, we showed that CT3.28H.BBζ functioned better than another GPC2 scFv, GPC2.19,[17] in the present CAR backbone, especially at lower E:T ratios and against NB lines with lower antigen densities (online supplemental figure 3) and better cell expansion and CAR persistence with tumor rechallenge (online supplemental figure 4). These data suggest that all three CAR constructs have a comparable function in vitro but that CT3.28H.BBζ lacks tonic signaling, which could positively impact antitumor activity in the context of persistent tumor exposure.

CT3.28H.BBζ demonstrates highly effective anti-NB activity in vivo

To determine which of the three GPC2-CAR constructs has the best antitumor activity against NB in vivo, we utilized an orthotopic PDX model. The 4–6 week-old NSG mice were injected orthotopically with SJNBL012407_X1. This PDX line has molecular features of high-risk NB

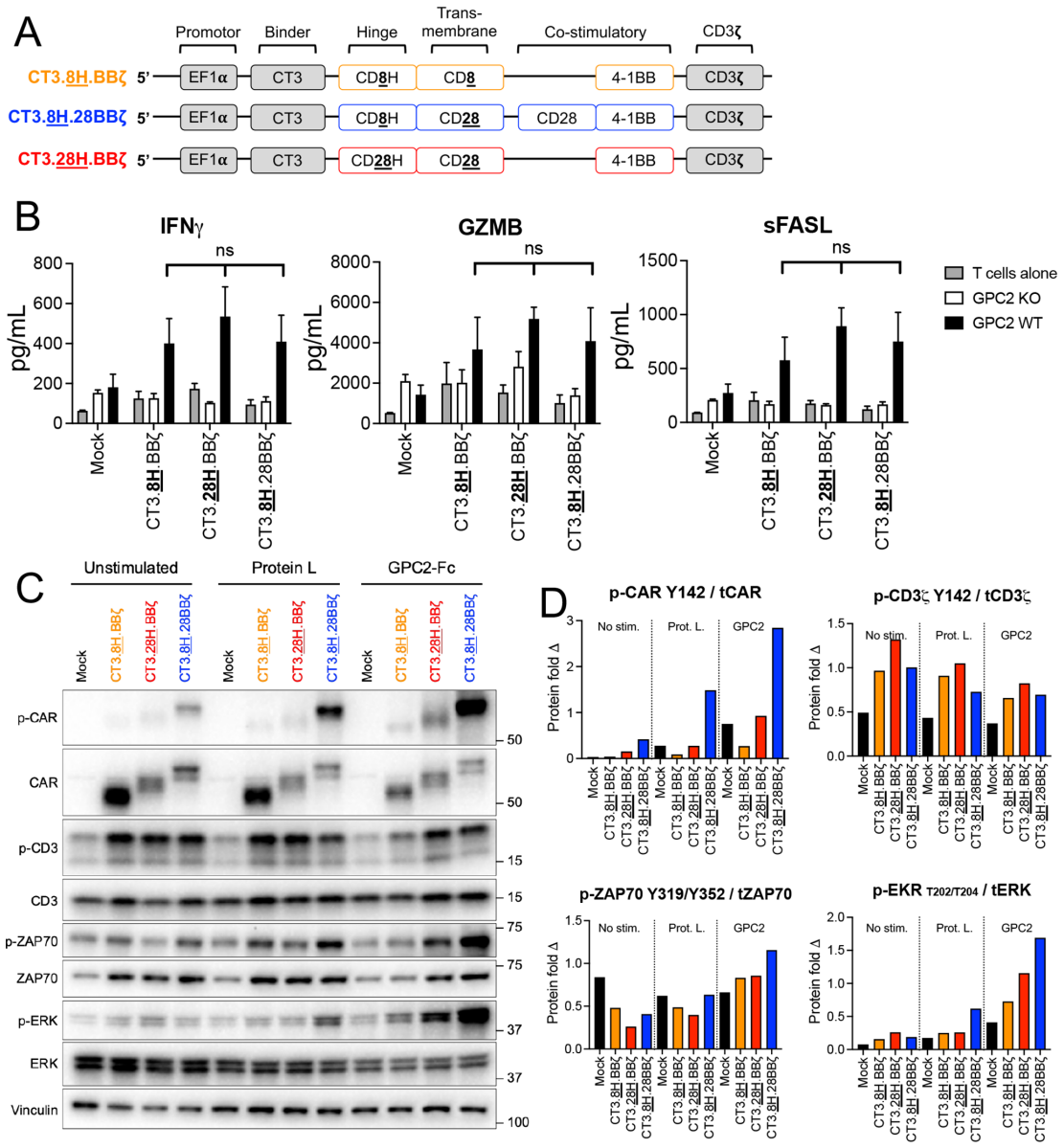

Figure 1 Comparison of three GPC2-CAR constructs in vitro. (A) Schema of the three CAR constructs used for preclinical studies with variable hinge, TM, and co-stimulatory domains. (B) Cytokine secretion profile of GPC2-CAR T cells at 24 hours in co-culture with tumor cells. Human T cells transduced with the three different GPC2-CARs were grown with GPC2-KO or GPC2-WT IMR-5 tumor cells. The levels of IFNγ, GZMB, and sFASL were significantly increased in the presence of GPC2 but comparable across the three tested CARs. (C) Western blot analysis to demonstrate CAR signaling in resting and CAR-crosslinked T cells. (D) Densiometric quantification of western blot signals from (C). CT3.8H.28BBζ shows prominent tonic signaling of the CAR at rest and a lack thereof in CT3.28H.BBζ and CT3.8H.BBζ. However, antigen-specific CAR activation induces higher phosphorylation levels in CT3.28H.BBζ compared with CT3.8H.BBζ. CAR, chimeric antigen receptor; GPC2, glypican-2; GZMB, granzyme B; IFN, interferon; KO, knock out; sFASL, soluble Fas ligand; TM, transmembrane; WT, wildtype

(*MYCN* amplification), and most tumor-bearing mice treated with conventional chemotherapy and/or immunotherapy cannot be cured.[32 33] Three weeks after tumor implantation, mice were randomized to receive either UT mock T cells or 2.5×10^6 CAR$^+$ T cells. Four weeks post CAR T cell infusion (Day 50 post tumor implantation), CT3.28H.BBζ induced the most significant tumor regression comparing all three CAR constructs (figure 2A). Since CT3.8H.BBζ has been previously published by our group[19 20] and had comparable activity to CT3.8H.28BBζ, we focused on the two unpublished constructs, CT3.28H.BBζ and CT3.8H.28BBζ. We conducted survival studies and examined the in vivo tumor growth kinetics following GPC2-CAR T cell injection. The 4–6 weeks old NSG mice with orthotopic IMR-5.ffLUC-GFP tumors were treated with high (5×10^6) or low-dose (2.5×10^6) CAR T cells (figure 2B). After high-dose treatment with CT3.28H.BBζ, all animals demonstrated a steep decline in their BLI signal, ultimately approximating background levels (figure 2C). Mice treated with high-dose CT3.8H.28BBζ responded temporarily but were unable to maintain

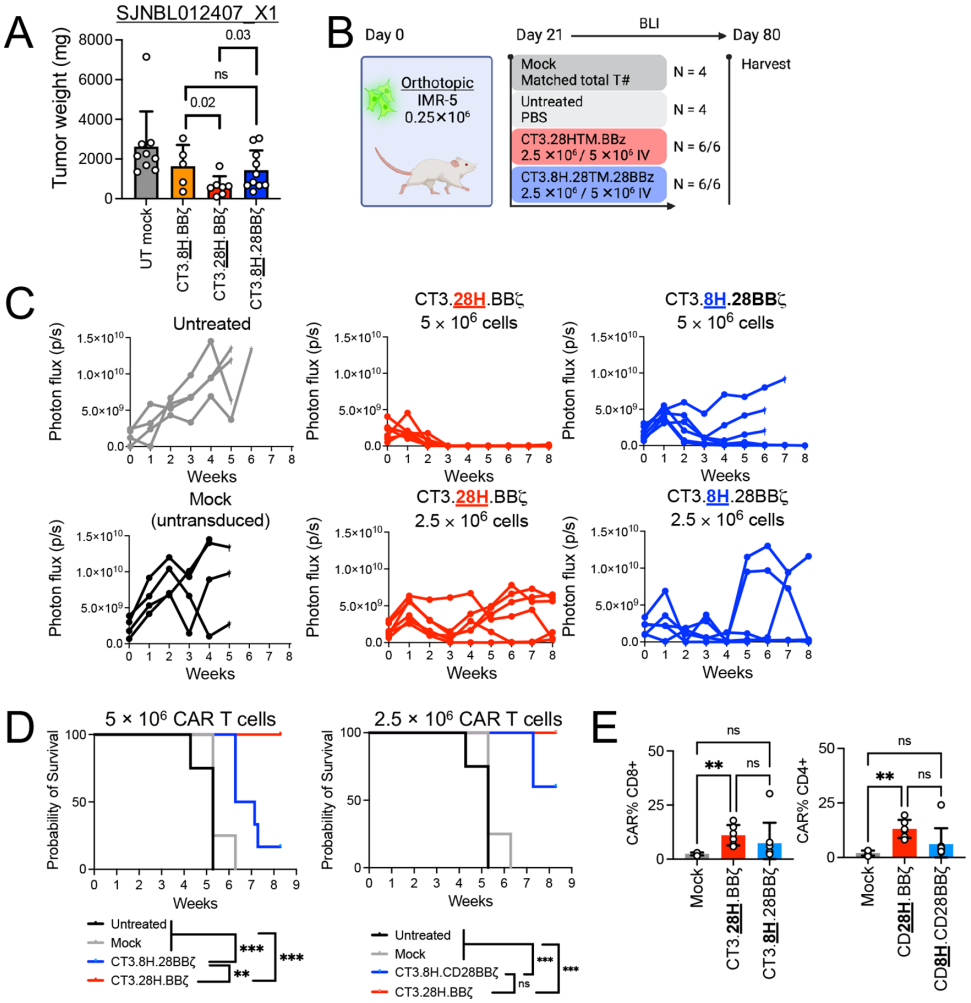

Figure 2 CT3.28H.BBζ outperforms CT3.8H.CD28BBζ in vivo. (A) Tumor weights on Day 50 post tumor injection. CT3.28H.BBζ induced the most significant tumor regression across all therapy groups. (B) Model system and experimental regimen. (C) Longitudinal BLI signals of mice treated with UT mock T cells or untreated controls and GPC2-targeted CAR T cells. Weekly BLI revealed that CT3.28H.BBζ-CAR T–treated animals demonstrated a profound decline in their BLI signal that was sustained for the duration of the study. In contrast, mice treated with CT3.8H.28BBζ or lower cell doses of each of the GPC2-targeted CAR T cells showed a temporary response but ultimately progressed. (D) Survival curves of mice from (C). (E) Persistence of CAR$^+$ T cells isolated from the tumor of treated mice in (C) on Day 80 by flow cytometry analysis. BLI, bioluminescence imaging; CAR, chimeric antigen receptor; GPC2, glypican-2; IV, intravenous; PBS, phosphate-buffered saline; UT, untransduced.

tumor control. All mice in both GPC2-CAR T cell groups treated with 2.5×10^6 CAR T cells demonstrated an initial decline in their BLI but eventually progressed with downregulation of GPC2 in relapsed tumors (online supplemental figure 5). The differences in the tumor growth kinetics between mice receiving the high and lower dose of CAR T cells were mirrored in the survival studies of these animals. Tumor-bearing mice treated with high-dose CT3.28H.BBζ CAR T cells exhibited the longest survival (figure 2D) and higher levels of tumor-infiltrating CAR$^+$ T cells by flow cytometry analysis (figure 2E; online supplemental figure 6). The survival between the CAR groups was not statistically different at the lower dose level. However, six of six mice never met the study endpoints when treated with CT3.28H.BBζ CAR T cells, while two of five treated with CT3.8H.28BBζ CAR T cells succumbed due to tumor. Although our in vitro experiments demonstrated a similar function of the three different GPC2-targeting CARs, the subsequent in vivo studies identified CT3.28H.BBζ as the most potent construct. The superior performance of CT3.28H.BBζ may be due to less tonic signaling, higher levels of CAR$^+$ effector cells in the tumor microenvironment (TME), and/or antigen escape (online supplemental figure 6). To further evaluate the molecular differences across the three CAR constructs, we next sought to analyze tumor-infiltrating T cells by single-cell RNA-seq.

CT3.28H.BBζ CAR T cells upregulate effector molecules in the TME

To understand the nature of the T cells expressing the different GPC2-CAR T constructs prior to infusion as well as after encountering tumor in vivo, we performed single-cell RNA-seq on the manufactured GPC2-CAR T as well as on harvested tumor-infiltrating T cells at Day 8, a time prior to tumor regression (typically occurs at Day 10).

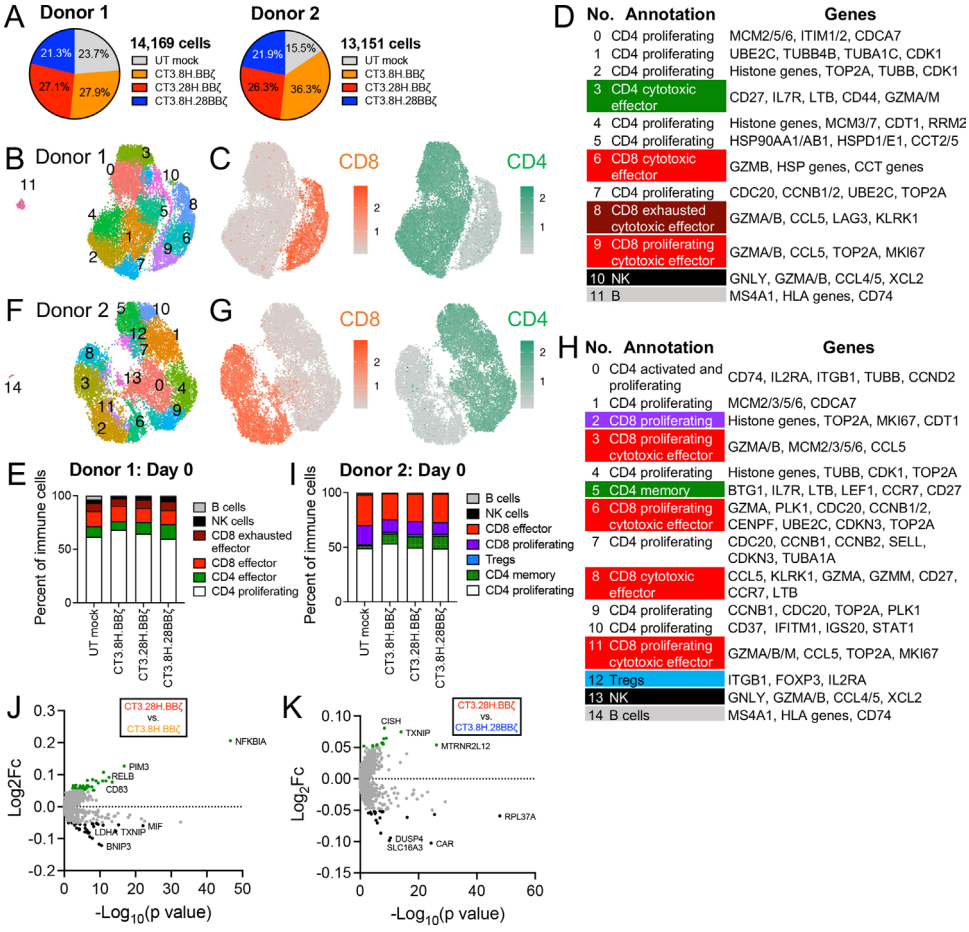

Figure 3 GPC2-CAR T cell manufacturing yields proliferating and cytotoxic effector T cells. (A) Proportions of captured immune cells on Day 8 of CAR T manufacturing. (B) UMAP, (C) CD8 and CD4 protein expression levels detected by TotalSeq, (D) cluster annotations, and (E) fractions of subsets of manufactured cells from Donor 1. (F) UMAP, (G) CD8 and CD4 protein expression levels, (H) cluster annotations, and (I) fractions of subsets of manufactured cells from Donor 2. (J) and (K) DEG analysis of the produced cells. CAR, chimeric antigen receptor; DEG, differentially expressed genes; GPC2, glypican-2; NK, natural killer; UMAP, uniform manifold approximation and projection; UT, untransduced

We manufactured CAR T cells from two donors and analyzed their transcriptomes prior to injection into the mice using the droplet-based 10X Genomics platform. After quality control and filtering, a total of 14,169 single-cell transcriptomes were obtained for Donor 1 and 13,515 for Donor 2 (figure 3A). Each subgroup was evenly represented for Donor 1, but more CT3.8H.BBζ cells and fewer UT mock cells were captured for Donor 2. To manually annotate the cellular subsets, we followed previously published annotation strategies.[34 35] We performed graph-based unsupervised clustering and used CD8 and CD4 protein expression and conventional genes to define T (*CD8A*, *CD4*), NK (*NKG7, GNLY*), and B cells (*MS4A1*). T cell subsets were further defined as cytotoxic effector cells by their robust expression of *PRF1* and various granzyme-encoding genes and memory cells by their expression of *SELL*, *IL7R*, CD27, and *LEF1* (online supplemental figure 7). Regulatory T cells (Tregs) were identified by *IL2RA* and *FOXP3*. Cell clusters were defined as proliferating when they expressed classic proliferation and cell cycle-related genes (eg, *TOP2A*, *MKI67*, *CCNB1/2*, minichromosome maintenance (MCM) complex, or histone genes).

The T cell injection product of Donor 1 was composed of 12 cell clusters (figure 3B), which were distinctly separated by their CD8 (22.3%) and CD4 (77.7%) protein expression (figure 3C). By using compound gene signatures, we found that this donor contained predominantly proliferating $CD8^+$ and $CD4^+$ T cells (72.8%) and $CD8^+$ cytotoxic effector cells (33.1%) at the end of the CAR T manufacturing process (figure 3D,E). A fraction of the $CD8^+$ cells were exhausted cytotoxic effector cells (figure 3D,E). Donor 2 consisted of 15 independent cell clusters (figure 3F). Like Donor 1, the total cell population contained fewer $CD8^+$ (37.9%) than $CD4^+$ T cells (62.1%; figure 3G) of which 25.6% were cytotoxic T cells and 1.7% Tregs (figure 3H,I).

To determine the ideal time point for single-cell RNA-seq analysis of the TME after T cell injection into mice, we evaluated the distribution and expansion of CAR T cells in vivo. To track the cells, we transduced GPC2-CAR T cells to express firefly luciferase-GFP (ffLUC-GFP). Three weeks following tumor implantation into the right adrenal gland fat pad, we injected GPC2-CAR-ffLUC-GFP T cells and conducted serial BLI. We found that T cells

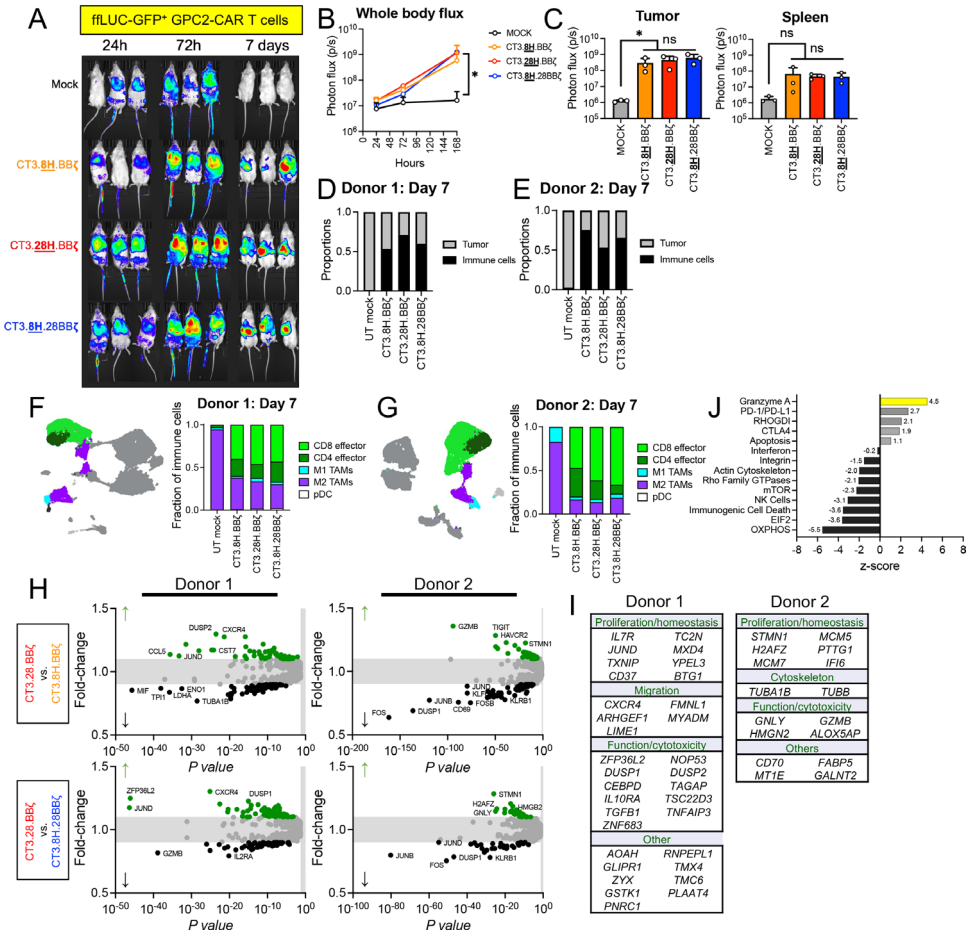

Figure 4 GPC2-CAR T cells home to the TME and enrich as cytotoxic effector population in vivo. (A) GPC2-targeted CAR T cell tracking using BLI in vivo. T cells were transduced to express ffLUC-GFP and were monitored serially for homing and expansion. (B–C) All three CARs enrich and expand in the TME compared with UT mock cells. *p<0.05; Student's t-test. (D–E) IMR-5–bearing mice underwent T cell injection. Eight days later, we isolated the tumors and performed single-cell RNA-seq. Quantifications of tumor and immune cells derived from the tumor are shown. (F–G) UMAP plots showing tumor cells (gray) and five immune subsets. The bar graphs quantify the immune proportions. (H) Volcano plots of differentially expressed genes comparing CT3.28H.BBζ vs CT3.8H.BBζ (top panels) and CT3.28H.BBζ vs CT3.8H.28BBζ (bottom panels). Green dots represent upregulated, black downregulated, and gray unchanged genes. (I) Differentially expressed genes grouped by function and extracted from both comparisons made in (H). (J) Compound pathway analysis reveals that CT3.28H.BBζ CAR T cells upregulate the granzyme A pathway but downregulate pathways related to mitochondrial oxidative phosphorylation (OXPHOS) and EIF2. BLI, bioluminescence imaging; CAR, chimeric antigen receptor; CTLA-4, cytotoxic T-lymphocytes-associated protein 4; EIF2, eukaryotic initiation factor 2; ffLUC, firefly luciferase; GFP, green fluorescent protein; GPC2, glypican-2; mTOR, mammalian target of rapamycin; NK, natural killer; TAM, tumor-associated macrophage; TME, tumor microenvironment; pDC, plasmacytoid dendritic cells; PD-1; programmed cell death protein-1; PD-L1, programmed death-ligand 1; seq, sequencing; UMAP, uniform manifold approximation and projection; UT, untransduced.

in all four test groups first accumulated in the lungs and femurs and gradually expanded over the next 48 hours (figure 4A). By Day 7, the overall BLI signal had faded in the UT mock T group, while all three GPC2-CAR groups demonstrated an increase in the signal confined to the tumor and spleen, consistent with local T cell expansion (figure 4B,C).

After CAR T-cell injection, tumors from IMR-5-bearing mice (Day 8) were found to contain large proportions of CD8 and CD4 effector T cells comprising approximately 50% or more of the cells from the TME (figure 4D–G). In contrast, UT mock cells accounted for <3% of the cells in the TME. This is consistent with the results from our in vivo tracking experiments, where UT mock T cells failed to expand and engraft (figure 4A). The residual cells in this group were almost exclusively M2 tumor-associated macrophages. Tumor cells were distinguished from immune cells by their gene expression and copy number variation profile (online supplemental figure 8).

Trajectory analysis of the immune cells in vivo revealed that the few numbers of antigen-presenting cells present at the time of injection were soon outnumbered by CD4 and CD8 T cells. These cells developed from a state of high proliferative capacity (marked by expression of *MKI67*) to terminally differentiated and dysfunctional *CD69*-expressing, *EOMES*-expressing, and *TOX*-expressing effector cells or transitioned to a memory phase evident by expression abundance of *IL7RA*, *LEF1*,

and *CCL5* (online supplemental figures 9–10). To better characterize the transcriptome of tumor-infiltrating CD8$^+$ effector cells across the GPC2-CAR T cell groups, we compared the gene expression profile of CT3.28H.BBζ with that of the two other GPC2-targeted CARs (figure 4H). In Donor 1, we found 33 differentially expressed genes (DEGs) that were shared by both analyses (ie, CT3.28H.BBζ vs CT3.8H.BBζ and CT3.28H.BBζ vs CT3.8H.28BBζ; figure 4I). In Donor 2, there were 16 shared DEGs (figure 4I). Compared with the other two CAR T cell groups, CT3.28H.BBζ CAR T cells exhibited upregulation of *CXCR4*, *ARHGEF1*, and *LIME1*, which are implied in chemokine-related T cell migration and T cell renewal.[36–38] Other DEGs include *IL7R*, *JUND*, *ZFP36L*, and *TXNIP*, which are important in T-cell homeostasis and memory formation.[39–43] CT3.28H.BBζ CAR T cells also had upregulated genes encoding effector molecules (eg, *GNLY*, *GZMB*, *ZNF683*, and *HMGN2*) and cell cycle components (eg, *STMN1*, *MCM5*, *MCM7*, and *PTTG1*). Lastly, pathway analysis corroborated these findings, demonstrating activation of the granzyme A pathway (z-score: 4.54; p value=1.16E−35). Interestingly, CT3.28H.BBζ CAR T cells also showed a downregulation of the EIF2 (z-score: −3.628; p value=6.19E−54) and oxidative phosphorylation pathways (z-score: −5.53; p value=1.85E−56; figure 4J). Pairwise DEG analysis revealed that compared with the other two CARs, CT3.28H.BBζ already expressed genes important in the regulation of pathways of T cell exhaustion (eg, *NFKBIA, CISH*), genes that promote T cell activation and proliferation (eg, *CD83,TXNIP, LDHA*), and genes that may prevent apoptosis (eg, *MTRNR2L12*; figure 4J,K). These findings suggest that at the time of manufacturing these cells, there are already transcriptomic differences that may influence the divergent cytotoxic activity and survival of the cells in vivo.

Taken together, our findings demonstrate that all GPC2-targeted CAR T cells substantially expand towards a cytotoxic effector population in vivo. Furthermore, CT3.28H.BBζ CAR T cells upregulate effector molecules and genes involved in T cell migration and memory homeostasis. These findings may be responsible for the superior antitumor cytotoxicity we observed in mice treated with CT3.28H.BBζ CAR T cells compared with the other CAR therapy groups.

CT3.28H.BBζ outperforms K666.28H.BBζ with superior antitumor activity against GD2$^+$ GPC2^{low} NB

Previous CAR T cell trials in NB were conducted with K666-based and 14.18-scFv-based GD2-CAR T cells.[7 9–11] Although the trials reported tolerability, very few of the treated patients achieved objective responses. Next, we asked the question of how CT3.28H.BBζ compared in their function to existing CAR T-cell therapies targeting GD2. We aimed to compare the preclinical activity of the K666-based and 14.G2a-based GD2-targeting CARs[7] with that of CT3.28H.BBζ. To create comparable testing conditions, we cloned the scFv's into the identical CAR construct used for CT3.28H.BBζ and CT3.8H.BBζ and performed head-to-head comparisons with serial tumor rechallenges in vitro (online supplemental figure 11). Subsequently, we chose K666.28H.BBζ and further compared the anti-NB activity of CT3.28H.BBζ with that of K666.28H.BBζ in vitro and in vivo. The CAR T cells demonstrated comparable transduction efficiencies (figure 5A). We incubated ffLUC-GFP-expressing SJNBL012407_X1, IMR-5 (both *MYCN*-amplified), and SH-SY5Y (*MYCN*-WT) with CT3.28H.BBζ or K666.28H.BBζ CAR T cells at varying E:T ratios. These NB cells have different expression levels of GPC2 and GD2 (online supplemental figure 12). After 48 hours, we determined tumor cell lysis by applying a luciferase reporter assay (figure 5B). At an E:T ratio of 1:1, CT3.28H.BBζ CAR T cells showed superior anti-NB cytotoxic compared with K666.28H.BBζ CAR T cells against the GD2^{intermediate} GPC2^{low} PDX and GD2^{low} GPC2^{low} SH-SY5Y. The tumor lysis was comparable in GD2^{high} GPC2 ^{high} IMR-5 in both groups. Next, we expanded our testing to an in vitro tumor rechallenge model with SJNBL012407_X1. We measured the cytotoxic capacity of the two CARs at 24 hours, Day 4, and Day 7 following daily tumor rechallenges. Although CT3.28H.BBζ CAR T cells showed better anti-NB cytotoxicity at first, their activity gradually decreased over time, rendering K666.28H.BBζ CAR T cells superior on Day 7 (figure 5C). We next compared the antitumor activity of the two CARs in vivo. SJNBL012407_X1-bearing mice were injected with 5×10^6 CAR$^+$ T cells on Day 21 after tumor inoculation. On Day 50 post tumor injection, we weighed the primary tumors and analyzed the bone marrow for residual NB cells. Interestingly, tumor weights were smaller after therapy with CT3.28H.BBζ CAR T cells compared with K666.28H.BBζ CAR T (figure 5D,E). Furthermore, we found that 3 out of 5 mice with K666.28H.BBζ CAR T cells had higher levels of detectable tumor cells in their bone marrow than all mice treated with CT3.28H.BBζ CAR T cells (figure 5F). A possible cause for therapy resistance after K666.28H.BBζ CAR T therapy could be the downregulation of GD2 in the primary tumors (online supplemental figure 13). Altogether, our findings demonstrate that CT3.28H.BBζ CAR T cells outperformed K666.28H.BBζ CAR T within an early time window in vitro as well as in an orthotopic NB-PDX in vivo model, leading to better tumor control of the primary tumor and a trend toward better control of metastatic disease burden in the bone marrow.

DISCUSSION

Previously, we have identified a unique scFv, CT3, that targets GPC2.[18 19] In this study, we conducted a systematic optimization of the GPC2-targeted CAR and demonstrated that CT3 integrated into a CAR backbone with a CD28 hinge and TM domain and 4-1BB co-stimulatory domain elicited the most potent preclinical activity against NB compared with other tested CAR backbones. Furthermore, we showed that CT3.28H.BBζ outperformed a clinical GD2-CAR, K666.28H.BBζ, in vivo. Given the robust

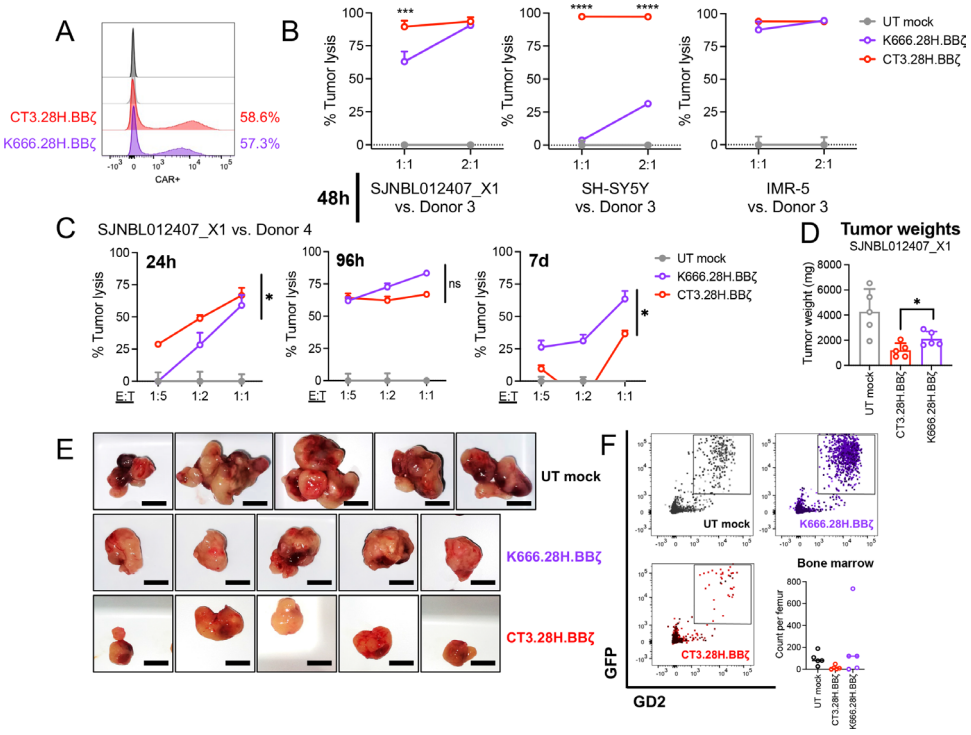

Figure 5 Head-to-head comparison of the GPC2-CAR (CT3.28H.BBζ) versus a GD2-CAR (K666.28H.BBζ). (A) Transduction efficiencies of CT3.28H.BBζ and K666.28H.BBζ CAR T cells. (B) In vitro cytotoxicity assays testing both CARs against three NB lines at varying E:T ratios. ***p<0.001; ****p<0.0001; two-way analysis of variance. (C) In vitro tumor rechallenge assay. CAR T cells are rechallenged every 24 hours. The cytotoxic activity is measured at 24 hours, 96 hours, and 7 days. *p<0.05; paired t-test. (D) Tumor weights on Day 50 post tumor implantation. *p<0.05; Student's t-test. (E) Images of harvested tumors on Day 50 post-implantation. Scale bar=1.0 cm. (F) Flow analysis of bone marrow cells derived from one femur. Tumor cells are identified as hCD45$^-$ mCD45$^-$ GD2$^+$ GFP$^+$ cells. The total cell number per femur is plotted, and each dot represents one mouse. CAR, chimeric antigen receptor; d, days; E:T, effector-to-tumor; GFP, green fluorescent protein; GPC2, glypican-2; h, hours; NB, neuroblastoma; UT, untransduced.

preclinical activity of CT3.28H.BBζ, these promising results require confirmation in the clinical context.

To date, clinical studies of adoptive cellular therapies in NB have focused on GD2-CAR T cells. Although all 14.18-based and K666-scFv-based GD2-CAR T cell trials reported tolerability and an explicit absence of neurotoxicity (a concern as GD2 is expressed at high levels not only in NB but also in peripheral nerves and the brain), disappointingly, only 3 of the cumulative 42 treated patients achieved objective responses.[7 9–11] This lack of efficacy was noted not only in first-generation but also in second-generation and third-generation GD2-CAR T cells and suggests that other targets or more refined CAR engineering may be necessary to increase the efficacy of CAR T cells against NB.

The lack of tumor-associated antigens in solid tumors has impeded the development of effective and safe CAR T cell therapies. GPC2 is a relatively new and unique target in NB. Three centers in the USA (ie, NCI, Stanford University, and the University of Pennsylvania) currently develop GPC2-CAR T cells. Critically, each of the three cell products that are in development has unique scFvs and differing CAR structures that may ultimately lead to varying antitumor activity and tolerability in the clinic, warranting the clinical testing of each CAR product.[16–19]

A recent publication described a GPC2-targeted CAR with a CD28ζ co-stimulatory domain that had limited efficacy against low-antigen density, which was mitigated through overexpression of cJUN.[17] Here, we demonstrate that optimization of our CAR leads to robust activity even against tumor cells with low GPC2 expression. Our scFv was derived from CT3 (patent number: 11066479), a high-affinity murine monoclonal antibody against human GPC2 obtained by immunization in C57BL/6 mice with a dissociation constant (KD) value of 0.5 nM. It binds to a conformational epitope that requires exon 3 and exon 10 of GPC2, which are spatially adjacent to each other based on electron microscopic structure analysis of the CT3 Fab and GPC2 3D complex.[19] Exon 3 is a unique sequence predominantly expressed in NB tumors but undetectable in most healthy tissues. The GPC2.D3-IgG1 antibody was originally isolated from a human Fab phage-displayed library with an affinity to human GPC2 of 0.2 nM.[16] The GPC2.19 human antibody was isolated from the same Fab phage-displayed library. GPC2.19 and GPC2.D3 share overlapping epitopes including residues 396–400. However, the former has a binding affinity to human GPC2 that is 11 nM, that is, 55-fold less than GPC2.D3. Lastly, the scFv sequence of CT3 is in variable fragment heavy chain (VH) and variable fragment light

chain (VL) VH-VL orientation with a (G4S)3 linker while GPC2.D3 and GPC2.19 exist in VL-VH orientation. Altogether, these differences may contribute to the differing binding properties of the scFv's. Because our scFv (CT3) targets the NB-associated exons 3 and 10,[19] CT3.28H.BBζ may have an even lower potential for on-target, off-tumor toxicities than anticipated. Additionally, the comparison between the CT3 and GPC2.19 scFv in our CAR backbone exhibited better cell expansion and cytotoxicity on tumor rechallenge, less expression of the exhaustion marker programmed cell death protein-1, and higher CAR persistence. Altogether, these findings may explain the functional differences between the two scFv's. Lastly, our preclinical head-to-head comparison with the GD2-targeted K666.28H.BBζ CAR suggests that the CT3.28H.BBζ CAR may improve on the low activity observed in clinical CAR T cell trials in NB.

Because the antigen density plays an important role in engaging the CAR and mediating a strong downstream signal for CAR activation[22] and given that GPC2 is expressed at relatively low levels in NB compared with other CAR targets,[17] we have applied iterative CAR engineering to develop the CT3.28H.BBζ CAR with robust cytotoxicity against NB. Factors like scFv affinity, epitope specificity, and CAR components such as the hinge, TM, and costimulatory domains can modulate the structural plasticity of CARs. Therefore, optimization of these components can be critical in relaying and amplifying scFv-antigen-binding and downstream CAR signaling for optimal CAR activation and CAR T-cell function.[44 45] We found the least tonic signaling and sustained anti-NB activity by using a CD28 hinge and TM domain and 4-1BB costimulatory domain. Furthermore, we discovered a differential upregulation of genes implied in effector function, trafficking, and memory formation associated with CT3.28H.BBζ. These observations underline the intricate relationship between CAR design and the cellular state and function of T cells and argue for careful CAR engineering and testing in the preclinical setting to optimally leverage engineered T cells for cellular therapies.

Lastly, we acknowledge that our mechanistic interrogations with single-cell RNA-seq were conducted at one point in time and may not fully capture the spectrum of molecular differences of the different CAR constructs. Furthermore, the mouse models with NSG mice and human PDX/cell lines and T cells eventually led to the occurrence of xenogeneic graft-versus-host disease (GVHD) and limited our ability to conduct long-term survival studies, which are useful to determine the role of CT3.28H.BBζ in immune surveillance and study mechanisms of late CAR T-cell resistance. Future preclinical studies may use NSG mice that lack murine major histocompatibility complex class I and II, which substantially decreases the occurrence of xenogeneic GVHD and could enable such experiments.

In summary, we applied stringent preclinical efficacy models to determine the anti-NB activity of the GPC2-targeted CAR and conducted mechanistic studies to support these observations. Our study has identified CT3.28H.BBζ as a lead GPC2-targeted CAR for further clinical development in children with NB. Additionally, preclinical testing in other GPC2-expressing childhood malignancies may be warranted to expand this therapy to patients with other pediatric solid tumors.

Twitter Mitchell Ho @MitchellHo

Acknowledgements We thank the National Cancer Institute (NCI) Center for Cancer Research (CCR) Animal Resource Program/NCI Biological Testing Branch (Dr M Custer and K Divi) for providing mice for our experiments, the NIH CC Blood bank (Thomas Lewis) for providing healthy donor blood cells, the Biological Resources Branch at the Frederick National Laboratory for giving us cytokines, Drs Z Liu and J Gulley for reviewing the article and giving us thoughtful suggestions, Dr A Mendoza for his assistance with animal regulatory work, J Buckley for his assistance with animal work, Dr S Heitzeneder for providing cell lines, Drs D Dimitrov and D Jelev for providing D3-IgG1 antibody, and the Children's Solid Tumor Network for providing the patient-derived xenograft line for our studies. Some figures were generated with Biorender.com.

Contributors MS: data curation, data analysis, manuscript review/editing; YC: computational analysis, manuscript review/editing; RO: data curation, data analysis, manuscript review/editing; JMR-G: data curation, manuscript review/editing; HGS: data curation, manuscript review/editing; HQ: manuscript review/editing; NL: data curation, manuscript review/editing; CS: data curation, manuscript review/editing; MCK: conceptualization, manuscript review/editing; ER: resources, manuscript review/editing; MH: conceptualization, funding acquisition, resources, manuscript review/editing; CJT: conceptualization, data analysis, funding acquisition, resources, manuscript review/editing; RN: conceptualization, resources, data curation, formal analysis, funding acquisition, validation, investigation, visualization, methodology, original draft.Guarantor: RN

Funding This work was supported by the Intramural Research Program of the National Institutes of Health, National Cancer Institute (NCI), Center for Cancer Research (CCR; ZIA BC 012066 to RN and ZIA BC 010788 to CJT), the US Department of Defense Peer Reviewed Cancer Research Program (CA191207 to RN), and the Cancer Moonshot Program through the NCI CCR Center for Cell-Based Therapy of the National Institutes of Health (all authors). The CCR Single Cell Analysis Facility was funded by the Frederick National Laboratory for Cancer Research (75N91019D00024). This work used the computational resources of the NIH HPC Biowulf cluster (http://hpc.nih.gov).

Competing interests None declared.

Patient consent for publication Not applicable.

Ethics approval Not applicable.

Provenance and peer review Not commissioned; externally peer reviewed.

Data availability statement Data are available in a public, open access repository. Data are available upon reasonable request. All data relevant to the study are included in the article or uploaded as supplementary information.

ORCID iDs
Eytan Ruppin http://orcid.org/0000-0003-4299-7657
Rosa Nguyen http://orcid.org/0000-0001-5143-2055

REFERENCES

1 Ries LAG SM, Gurney JG, Linet M, *et al*. *Cancer incidence and survival among children and adolescents: United States seer program 1975-1995*. Bethesda, MD, NIH: National Cancer Institute, SEER Program, n.d.
2 Matthay KK, Villablanca JG, Seeger RC, *et al*. Treatment of high-risk neuroblastoma with intensive chemotherapy, radiotherapy, autologous bone marrow transplantation, and 13-cis-retinoic acid. children's cancer group. *N Engl J Med* 1999;341:1165–73.
3 Yu AL, Gilman AL, Ozkaynak MF, *et al*. Long-Term follow-up of a phase III study of ch14.18 (Dinutuximab) + cytokine immunotherapy in children with high-risk neuroblastoma: COG study ANBL0032. *Clin Cancer Res* 2021;27:2179-2189.
4 Maude SL, Frey N, Shaw PA, *et al*. Chimeric antigen receptor T cells for sustained remissions in leukemia. *N Engl J Med* 2014;371:1507–17.
5 Maude SL, Laetsch TW, Buechner J, *et al*. Tisagenlecleucel in children and young adults with B-cell lymphoblastic leukemia. *N Engl J Med* 2018;378:439–48.
6 Hou AJ, Chen LC, Chen YY. Navigating CAR-T cells through the solid-tumour microenvironment. *Nat Rev Drug Discov* 2021;20:531–50.
7 Straathof K, Flutter B, Wallace R, *et al*. Antitumor activity without on-target off-tumor toxicity of GD2-chimeric antigen receptor T cells in patients with neuroblastoma. *Sci Transl Med* 2020;12:eabd6169.
8 Heczey A, Courtney AN, Montalbano A, *et al*. Anti-GD2 CAR-NKT cells in patients with relapsed or refractory neuroblastoma: an interim analysis. *Nat Med* 2020;26:1686–90.
9 Heczey A, Louis CU, Savoldo B, *et al*. Car T cells administered in combination with Lymphodepletion and PD-1 inhibition to patients with neuroblastoma. *Mol Ther* 2017;25:2214–24.
10 Louis CU, Savoldo B, Dotti G, *et al*. Antitumor activity and long-term fate of chimeric antigen receptor-positive T cells in patients with neuroblastoma. *Blood* 2011;118:6050–6.
11 Pule MA, Savoldo B, Myers GD, *et al*. Virus-specific T cells engineered to coexpress tumor-specific receptors: persistence and antitumor activity in individuals with neuroblastoma. *Nat Med* 2008;14:1264–70.
12 Moghimi B, Muthugounder S, Jambon S, *et al*. Preclinical assessment of the efficacy and specificity of GD2-B7H3 SynNotch CAR-T in metastatic neuroblastoma. *Nat Commun* 2021;12:511.
13 Walker AJ, Majzner RG, Zhang L, *et al*. Tumor antigen and receptor densities regulate efficacy of a chimeric antigen receptor targeting anaplastic lymphoma kinase. *Mol Ther* 2017;25:2189–201.
14 Crossland DL, Denning WL, Ang S, *et al*. Antitumor activity of CD56-chimeric antigen receptor T cells in neuroblastoma and SCLC models. *Oncogene* 2018;37:3686–97.
15 Künkele A, Taraseviciute A, Finn LS, *et al*. Preclinical assessment of CD171-Directed CAR T-cell adoptive therapy for childhood neuroblastoma: CE7 epitope target safety and product manufacturing feasibility. *Clin Cancer Res* 2017;23:466–77.
16 Bosse KR, Raman P, Zhu Z, *et al*. Identification of GPC2 as an oncoprotein and candidate immunotherapeutic target in high-risk neuroblastoma. *Cancer Cell* 2017;32:295–309.
17 Heitzeneder S, Bosse KR, Zhu Z, *et al*. GPC2-CAR T cells tuned for low antigen density mediate potent activity against neuroblastoma without toxicity. *Cancer Cell* 2022;40:53–69.
18 Li N, Fu H, Hewitt SM, *et al*. Therapeutically targeting glypican-2 via single-domain antibody-based chimeric antigen receptors and immunotoxins in neuroblastoma. *Proc Natl Acad Sci U S A* 2017;114:E6623–31.
19 Li N, Torres MB, Spetz MR, *et al*. CAR T cells targeting tumor-associated exons of glypican 2 regress neuroblastoma in mice. *Cell Rep Med* 2021;2:100297.
20 Tian M, Cheuk AT, Wei JS, *et al*. An optimized bicistronic chimeric antigen receptor against GPC2 or CD276 overcomes heterogeneous expression in neuroblastoma. *J Clin Invest* 2022;132:e155621.
21 Filmus J, Capurro M, Rast J. Glypicans. *Genome Biol* 2008;9:224.
22 Majzner RG, Rietberg SP, Sotillo E, *et al*. Tuning the antigen density requirement for CAR T-cell activity. *Cancer Discov* 2020;10:702–23.
23 Li N, Nguyen R, Thiele CJ, *et al*. Preclinical testing of chimeric antigen receptor T cells in neuroblastoma mouse models. *STAR Protoc* 2021;2:100942.
24 Pule MA, Savoldo B, Myers GD, *et al*. Virus-Specific T cells engineered to coexpress tumor-specific receptors: persistence and antitumor activity in individuals with neuroblastoma. *Nat Med* 2008;14:1264–70.
25 Nguyen R, Houston J, Chan WK, *et al*. The role of interleukin-2, all-trans retinoic acid, and natural killer cells: surveillance mechanisms in anti-GD2 antibody therapy in neuroblastoma. *Cancer Immunol Immunother* 2018;67:615–26.
26 Wolock SL, Lopez R, Klein AM. Scrublet: computational identification of cell doublets in single-cell transcriptomic data. *Cell Syst* 2019;8:281–91.
27 Stuart T, Butler A, Hoffman P, *et al*. Comprehensive integration of single-cell data. *Cell* 2019;177:1888–902.
28 Hao Y, Hao S, Andersen-Nissen E, *et al*. Integrated analysis of multimodal single-cell data. *Cell* 2021;184:3573–87.
29 Aran D, Looney AP, Liu L, *et al*. Reference-based analysis of lung single-cell sequencing reveals a transitional profibrotic macrophage. *Nat Immunol* 2019;20:163–72.
30 Tickle TL, Tirosh I, Georgescu C, *et al*. *inferCNV of the Trinity CTAT project*. Cambridge, MA, USA: Klarman Cell Observatory, Broad Institute of MIT and Harvard, 2019.
31 Krämer A, Green J, Pollard J, *et al*. : . Causal analysis approaches in ingenuity pathway analysis. *Bioinformatics* 2014;30:523–30. Jr.
32 Nguyen R, Wang H, Sun M, *et al*. Combining selinexor with alisertib to target the p53 pathway in neuroblastoma. *Neoplasia* 2022;26:100776.
33 Nguyen R, Zhang X, Sun M, *et al*. Anti-Gd2 antibodies conjugated to IL15 and IL21 mediate potent antitumor cytotoxicity against neuroblastoma. *Clin Cancer Res* 2022;28:3785–96.
34 Wilson TL, Kim H, Chou C-H, *et al*. Common trajectories of highly effective CD19-specific CAR T cells identified by endogenous T-cell receptor lineages. *Cancer Discov* 2022;12:2098–119.
35 Patil VS, Madrigal A, Schmiedel BJ, *et al*. Precursors of human $CD4^+$ cytotoxic T lymphocytes identified by single-cell transcriptome analysis. *Sci Immunol* 2018;3:eaan8664.
36 Bouafia A, Lofek S, Bruneau J, *et al*. Loss of Arhgef1 causes a human primary antibody deficiency. *J Clin Invest* 2019;129:1047–60.
37 Chaix J, Nish SA, Lin W-HW, *et al*. Cutting edge: CXCR4 is critical for CD8+ memory T cell homeostatic self-renewal but not rechallenge self-renewal. *J Immunol* 2014;193:1013–6.
38 Park I, Son M, Ahn E, *et al*. The transmembrane adaptor protein lime is essential for chemokine-mediated migration of effector T cells to Inflammatiory sites. *Mol Cells* 2020;43:921–34.
39 Schluns KS, Kieper WC, Jameson SC, *et al*. Interleukin-7 mediates the homeostasis of naïve and memory CD8 T cells in vivo. *Nat Immunol* 2000;1:426–32.
40 Meixner A, Karreth F, Kenner L, *et al*. Jund regulates lymphocyte proliferation and T helper cell cytokine expression. *Embo J* 2004;23:1325–35.
41 Ruppert SM, Chehtane M, Zhang G, *et al*. JunD/AP-1-mediated gene expression promotes lymphocyte growth dependent on interleukin-7 signal transduction. *PLoS One* 2012;7:e32262.
42 Muri J, Thut H, Kopf M. The thioredoxin-1 inhibitor TXNIP restrains effector T-cell and germinal center B-cell expansion. *Eur J Immunol* 2021;51:115–24.
43 Petkau G, Mitchell TJ, Chakraborty K, *et al*. The timing of differentiation and potency of CD8 effector function is set by RNA binding proteins. *Nat Commun* 2022;13:2274.
44 Alabanza L, Pegues M, Geldres C, *et al*. Function of novel anti-CD19 chimeric antigen receptors with human variable regions is affected by hinge and transmembrane domains. *Mol Ther* 2017;25:2452–65.
45 Chen X, Mirazee JM, Skorupka KA, *et al*. The CD8α hinge is intrinsically disordered with a dynamic exchange that includes proline cis-trans isomerization. *J Magn Reson* 2022;340:107234.